

Entanglement transitions in the quantum Ising chain: A comparison between different unravelings of the same Lindbladian

Giulia Piccitto,¹ Angelo Russomanno,² and Davide Rossini¹

¹ Dipartimento di Fisica dell’Università di Pisa and INFN, Largo Pontecorvo 3, I-56127 Pisa, Italy

² Scuola Superiore Meridionale, Università di Napoli Federico II Largo San Marcellino 10, I-80138 Napoli, Italy

We study the dynamics of entanglement in the quantum Ising chain with dephasing dissipation in a Lindblad master equation form. We consider two unravelings which preserve the Gaussian form of the state, allowing to address large system sizes. The first unraveling gives rise to a quantum-state-diffusion dynamics, while the second one describes a specific form of quantum-jump evolution, suitably constructed to preserve Gaussianity. In the first case we find a crossover from area-law to logarithm-law entanglement scaling and draw the related phase diagram. In the second case we only find logarithm-law scaling, remarking the different entanglement behavior for different unravelings of the same Lindblad equation. Finally, we compare these outcomes with the predictions of a non-Hermitian Hamiltonian evolution, finding conflicting results.

I. INTRODUCTION

Understanding the physics of quantum systems coupled to an external environment is intriguing both for applications in recent quantum technologies and from a fundamental perspective, being related to the boundary between classical and quantum domains [1–3]. In the hypothesis of a weak and Markovian coupling with the bath, the underlying dynamics can be reliably described by a master equation in the Lindblad form [4–6] for the reduced density matrix of the system. Recently it has been argued that this framework can also model the process of quantum measuring at random or continuous times. In fact, the external environment can be thought as a measurement apparatus performing measurements on the quantum system [7, 8]. While the measurement process itself is stochastic and the outcome is a pure-state quantum trajectory, the density matrix obtained by averaging over such trajectories obeys a Lindblad-type evolution.

Here we are interested in the effects of coupling with an environment on the entanglement dynamics in quantum many-body systems [9], a crucial property for quantum computing purposes [10]. In particular, we focus on the so-called measurement-induced entanglement transitions: When measuring a quantum many-body system, the interplay between the unitary dynamics (contributing to the creation of entanglement) and the quantum measurements (contributing to its destruction) might result in sharp transitions between different dynamical phases, characterized by qualitatively different entanglement properties in the asymptotic regime [11–22].

A paradigmatic example is provided by random circuits undergoing random measurements [23–43], which may display a transition between a phase with volume-law scaling of entanglement and another phase with area-law scaling. In the case of free-fermion Hamiltonians, the asymptotic volume-law of the unitary evolution [44–46] is unstable for any measurement rate and exhibits a transition towards a subextensive phase [11, 12, 20, 22]. Similar results have been obtained for free-fermion random circuits with temporal randomness [47], a setting that has

been recently generalized to higher dimensions [48], Majorana random circuits [18, 49], and Dirac fermions [50]. These entanglement transitions can sometimes be predicted by a related non-Hermitian Hamiltonian evolution, as discussed in Ref. [51] for a quantum Ising chain with no transverse field.

The set of stochastic trajectories whose average gives rise to a Lindblad evolution (unraveling) depends on the physics of the involved measurement process [8]. A question which has been only marginally addressed so far is related to the observation that any Lindblad equation has many possible unravelings. The entanglement properties are encoded in the stochastic quantum trajectories, that, contrarily to the average density matrix, contain only quantum correlations. One expects these correlations to strongly depend on the specific unraveling. In fact, each unraveling corresponds to a specific measurement process and a specific way for destroying the entanglement generated by the unitary part of the dynamics. This can give rise to different dynamical phases and entanglement transitions. An example of that is provided in Ref. [11], where the unitary unraveling gives rise to a volume-law asymptotic entanglement, while the quantum state diffusion one provides an area-law entanglement.

In this paper we study measurement-induced quantum transitions in the transverse-field quantum Ising chain undergoing a dephasing measurement process. We consider two different unravelings: first we solve the quantum-state-diffusion stochastic Schrödinger equation, then we consider an unraveling based on a quantum-jump measurement process. The phase diagram in Fig. 1, obtained by solving the quantum-state-diffusion dynamics, extends the results of Ref. [51] to the case of non-zero transverse field. We find the existence of a crossover point from a subextensive to an area-law phase that depends on the measurement and the field strength; the subextensive region reduces while increasing the system size. For small couplings with the measurement apparatus, we observe the emergence of a maximum in the asymptotic entanglement entropy close to the zero-temperature quantum critical point, as a reminiscence of the unitary dynamics.

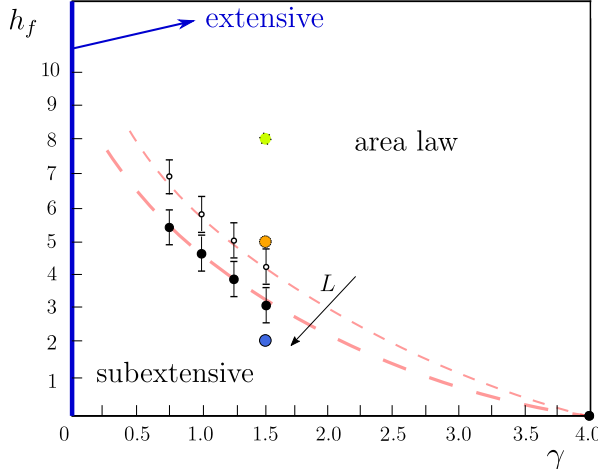


FIG. 1. Sketchy phase diagram of the measurement-induced entanglement transition in the quantum Ising chain, obtained by solving the quantum-state-diffusion dynamics. Here γ denotes the measurement rate, while h_f the transverse-field strength. The line $\gamma = 0$ corresponds to the singular limit of the unitary dynamics, where the asymptotic entanglement entropy obeys a volume-law scaling (i.e., it grows proportionally to the system size L). For $\gamma > 0$, the entanglement is either subextensive (i.e., it scales $\propto \log L$) or it follows an area-law scaling (i.e., it is independent of L). The crossover between these two regimes occurs at a threshold value of h_f which strongly depends on the system size and on the measurement rate. Black dots with errorbars denote the threshold fields evaluated at $L_{\max} = 256$ (big filled circles) and $L_{\max} = 192$ (small empty circles). Red dashed lines are guides to the eye. The blue, orange, and light-green circles mark the parameters used for simulating the quantum trajectories dynamics in Fig. 5. Even though some of the parameters have been chosen deep in the area-law phase, with this unraveling, the entanglement entropy always exhibits a logarithmic growth with L .

We then compare these results with those obtained from the quantum-jump measurement process. To this purpose, we choose slightly different measurement operators, which preserve the Gaussian form of the state (allowing numerics for quite large system size) and at the same time result in the same Lindblad equation. With this unraveling we do not find any entanglement entropy transition, not even in the parameter range where the quantum state diffusion predicts it. In fact, we monitor the entanglement trajectories at fixed $\gamma = 1.5$, for $h_f = 2, 5, 8$, marked in Fig. 1 by the blue, orange, and light-green circle, respectively, and always observe a subextensive growth with L . However we should stress that, considered the size-dependence of the crossover point and the computational effort needed for simulations, it is not possible to completely rule out the existence of an area-law phase from a numerical analysis. Finally, we compare both unravelings with the non-Hermitian Hamiltonian dynamics and find no agreement with this approximate dynamics.

The paper is organized as follows. In Sec. II we introduce the model, the two unravelings, and the way they preserve the Gaussianity of the state in each quantum trajectory. In Sec. III we discuss our results on the quantum-state-diffusion unraveling, in particular its phase diagram. In Sec. IV we present the logarithm-law behavior of the asymptotic entanglement in the quantum-jump unraveling. We also show that results with both unravelings cannot be predicted through a non-Hermitian Hamiltonian evolution. Finally, in Sec. V we draw our conclusions. The Appendix contains technical details that are useful for the numerical treatment of the dynamics of Gaussian fermionic systems in the presence of quantum measurements.

II. THEORETICAL FRAMEWORK

A. Hamiltonian model

We consider the integrable quantum Ising chain with L spins, described by the Hamiltonian

$$\hat{H} = -J \sum_{j=1}^L \hat{\sigma}_j^x \hat{\sigma}_{j+1}^x - h \sum_{j=1}^L \hat{\sigma}_j^z. \quad (1)$$

The spin-1/2 Pauli matrices $\hat{\sigma}_j^\alpha$ act on the j th site ($\alpha = x, y, z$), while J and h denote, respectively, the spin-spin coupling and the transverse magnetic-field strength. In what follows we set $J = 1$ as the energy scale, assume periodic boundary conditions ($\hat{\sigma}_{L+1}^\alpha \equiv \hat{\sigma}_1^\alpha$), and work in units of $\hbar = 1$. The Hamiltonian (1) features a parity symmetry generated by the operator $\hat{P} = \otimes_{j=1}^L \hat{\sigma}_j^z$, which divides the Hilbert space into two subspaces of dimension 2^{L-1} . The quantum Ising chain is known to exhibit a zero-temperature quantum phase transition from a paramagnetic state (for $h > h_c$) to a ferromagnetic state (for $h < h_c$), when the transverse-field strength crosses the critical value $h_c = 1$ and the above symmetry is broken [52]. Without loss of generality we restrict our analysis of the dynamics to the even parity sector.

The ground-state bipartite entanglement entropy of a subportion of the chain with ℓ sites obeys an *area-law* scaling (meaning that it is independent of ℓ , in one-dimension), except at the critical point, where it grows logarithmically with ℓ [46, 53]. On the other hand, during the unitary dynamics after a sudden quench in the transverse field h (or during a periodic driving [?]), it exhibits a linear growth in time eventually attaining an asymptotic constant value which increases linearly with ℓ (i.e., *volume-law* behavior, in one dimension) [45]. The asymptotic entanglement entropy as a function of h features a non-analytical cusp at h_c .

As explained in Appendix A, the above Ising chain (1) can be mapped into a quadratic spinless-fermion Hamiltonian. Using the Nambu spinor notation, $\hat{\Psi} = (\hat{c}_1, \dots, \hat{c}_L, \hat{c}_1^\dagger, \dots, \hat{c}_L^\dagger)^T$, with $\hat{c}_j^{(\dagger)}$ denoting anticommuting fermionic annihilation (creation) operators, such

Hamiltonian reads

$$\hat{H} = \frac{1}{2} \hat{\Psi}^\dagger \mathbb{H} \hat{\Psi} + \text{const.}, \quad (2)$$

where \mathbb{H} is the so-called Bogoliubov-De Gennes matrix defined in Eq. (A4). This can be easily diagonalized by performing a $2L \times 2L$ transformation \mathbb{U} such that

$$\mathbb{U}^{-1} \mathbb{H} \mathbb{U} = \text{diag}(\omega_k, -\omega_k). \quad (3)$$

For the Hamiltonian in Eq. (1), the dispersion relation is

$$\omega_k = 2J \sqrt{1 + (h/J)^2 - 2(h/J) \cos k}, \quad (4)$$

where the momenta $k = 2\pi n/L$, $n = -L/2 + 1, \dots, L/2$ are fixed by the parity sector we chose. This analysis will be useful in Sec. IV B, in the context of the non-Hermitian Hamiltonian approximation.

A similarly simple treatment is possible for a non-uniform model and for the nonequilibrium dynamics, provided $\mathbb{U}(t)$ in Eq. (3) depends on time and obeys the equation $i\partial_t \mathbb{U}(t) = \mathbb{H} \mathbb{U}(t)$ [54]. The key point is that, in the ground-state and the dynamical cases, the state of the system keeps the Gaussian form

$$|\psi\rangle = \mathcal{N} \exp \left(\frac{1}{2} \sum_{j_1 j_2=1}^L Z_{j_1 j_2} \hat{c}_{j_1}^\dagger \hat{c}_{j_2}^\dagger \right) |0\rangle, \quad (5)$$

where $Z = -(U^\dagger)^{-1} V^\dagger$ is a quadratic antisymmetric form [the U and V matrices being sub-blocks of \mathbb{U} , see Eq. (A7)], \mathcal{N} a normalization factor, and $|0\rangle$ the vacuum of the $\hat{c}_j^{(\dagger)}$ fermions [54]. This Gaussian form is preserved by the application of the exponential of any operator quadratic in $\hat{c}_j^{(\dagger)}$, as for the Hamiltonian (2). In the next subsection we show that the two unravelings we are going to consider amount precisely to the application to the state (5) of exponentials of operators quadratic in $\hat{c}_j^{(\dagger)}$. So the Gaussianity is preserved, together with the possibility of a simple numerical treatment, whose complexity scales polynomially with L .

B. The measurement process

The measurements of the environment give rise to a stochastic quantum dynamics. This means that the evolution of the state is provided by a trajectory $|\psi_t\rangle$ (also known as conditional state) that is the solution of a single realization of a stochastic process which models the quantum measurements. By ensemble averaging over the trajectories, we obtain the mean state $\bar{\rho}(t) \equiv \overline{|\psi_t\rangle \langle \psi_t|}$. Such mean state follows a Lindblad-type evolution, [55]

$$\frac{d}{dt} \bar{\rho}(t) = -i[\hat{H}, \bar{\rho}(t)] - \frac{\gamma}{2} \sum_j [\hat{m}_j [\hat{m}_j, \bar{\rho}(t)]], \quad (6)$$

where \hat{m}_j are the Hermitian measurement operators and γ quantifies the strength of the coupling between the system and the measurement apparatus. There are many

stochastic processes giving the same Lindblad-type evolution. In what follows we consider two different measurement processes that are the unraveling of the same Lindblad equation (6).

1. Quantum state diffusion with continuous measurements

We aim to measure the number of fermions on the j th site of the chain, hence we set $\hat{m}_j \equiv \hat{n}_j$, where $\hat{n}_j = \hat{c}_j^\dagger \hat{c}_j$ denotes the number operator. In this case, the Lindblad master equation is obtained by simply substituting $\hat{m}_j \mapsto \hat{n}_j$ in Eq. (6).

We start assuming the system to be *continuously* measured, i.e., the information is continually extracted from it and the strength of the measurements is proportional to a small time interval δt [56]. This can be obtained, for instance, by integrating the Schrödinger equation over δt ; Thanks to the Markov approximation, the resulting integrals of the couplings to the environment can be considered as Gaussian random variables, uncorrelated at different times [8]. In this setting (namely, the quantum-state-diffusion model) we can write the measured dynamics as a collection of Wiener processes resulting in a stochastic Schrödinger equation [see Eq. (B1) in App. B]. Discretizing the time, the approximate evolution of the state over one step δt of the dynamics is

$$|\psi_{t+\delta t}\rangle \simeq C e^{\sum_j [\delta W_t^j + (2\langle \hat{n}_j \rangle_t - 1)\gamma \delta t] \hat{n}_j} e^{-i\hat{H}\delta t} |\psi_t\rangle, \quad (7)$$

with δW_t^j being normal distributed variables with zero mean and variance $\gamma \delta t$, and $\langle \cdot \rangle_t = \langle \psi_t | \cdot | \psi_t \rangle$. To a good approximation, for small enough δt this Trotterized evolution faithfully describes the real dynamics [11] and preserves the Gaussianity of the state (for technical details, see Appendix B).

2. Quantum jumps

Another possibility we consider is an occasional, yet abrupt, measurement of the quantum state. This is what happens, for instance, to the electromagnetic field coupled to a photodetector. Namely, at each time interval, there is a chance for the state to be measured (i.e., the detector clicks) and projected, thus undergoing a so-called *quantum jump* [7]. An interpretation of this process is given by re-writing Eq. (6) as

$$\frac{d}{dt} \bar{\rho} = -i(\hat{H}_{\text{eff}} \bar{\rho} - \bar{\rho} \hat{H}_{\text{eff}}^\dagger) + \gamma \sum_j \hat{m}_j \bar{\rho} \hat{m}_j, \quad (8)$$

with

$$\hat{H}_{\text{eff}} = \hat{H} - i\frac{\gamma}{2} \sum_j \hat{m}_j^2. \quad (9)$$

The dynamics can be thought of as a deterministic non-Hermitian evolution driven by \hat{H}_{eff} plus a stochastic part

generated by the possibility of measuring \hat{m}_j . In order to preserve the Gaussian form of the state, we choose a slightly different form of the measurement operators

$$\hat{m}_j \mapsto (\hat{1} + \alpha \hat{n}_j), \quad (10)$$

with $\alpha > 0$ real and $\hat{1}$ being the identity operator. Substituting these operators in Eq. (8), we easily see that the Lindblad master equation has the form of Eq. (6) with \hat{m}_j given by $\alpha \hat{n}_j$. So, for $\alpha = 1$, the master equation is the same as in the quantum-state-diffusion case above, although the measurement operators are different. Now, defining the quantity

$$p_j = \gamma [1 + \alpha(\alpha + 2) \langle \hat{n}_j \rangle_t], \quad (11)$$

and discretizing the time with intervals δt , the quantum-jump evolution $|\psi_t\rangle \rightarrow |\psi_{t+\delta t}\rangle$ can be obtained by applying at each step δt

1. with probability $\pi_j = p_j \delta t$, the jump operator

$$|\psi_t\rangle \rightarrow \frac{(\hat{1} + \alpha \hat{n}_j)}{p_j} |\psi_t\rangle; \quad (12)$$

2. with probability $p = 1 - \sum_j \pi_j$, the evolution operator associated to non-Hermitian Hamiltonian $\hat{H}_{\text{eff}} = \hat{H} - \frac{i\gamma\alpha(2+\alpha)}{2} \sum_j \hat{n}_j^2$:

$$|\psi_t\rangle \rightarrow e^{-i\hat{H}_{\text{eff}}\delta t} |\psi_t\rangle. \quad (13)$$

Obviously, operation 2. preserves the Gaussianity, since \hat{H}_{eff} is quadratic in the $\hat{c}_j^{(\dagger)}$ fermions of Sec. II A. The same holds for operation 1., since the identity

$$\hat{1} + \alpha \hat{n}_j = e^{\log(1+\alpha)\hat{n}_j} \quad (14)$$

guarantees that the operator applied to $|\psi_t\rangle$ in (12) is the exponential of an operator which is quadratic in the $\hat{c}_j^{(\dagger)}$ fermions. As shown in Appendix C, if the measurement operators are \hat{n}_j , this dynamics is not guaranteed to not preserve Gaussianity, thus exponentially increasing the difficulty of its numerical treatment. Indeed, the simple application of \hat{n}_j gives rise to the superposition of two Gaussian states. After few jumps, the state would be a superposition of many Gaussian states, thus preventing a simple numerical treatment.

We conclude this section by remarking that the form of the quantum-jump operator in (10) is quite general. Indeed, due to the property $\hat{n}_j^2 = \hat{n}_j$ holding for spinless fermions, any operator of the form $\hat{O}_j = f(\hat{n}_j)$ can be written as $\hat{O}_j = [f(0)]\hat{1} + [f(1) - f(0)]\hat{n}_j$, which is the same as (10), provided that $f(0) \neq 0$ and $f(0) \neq f(1)$.

III. QUANTUM STATE DIFFUSION: RESULTS

We now present the results obtained under the assumption that the system is continuously monitored. As detailed below, the entanglement entropy $S_\ell(L)$ of a subsystem of size ℓ undergoes a measurement-induced transition

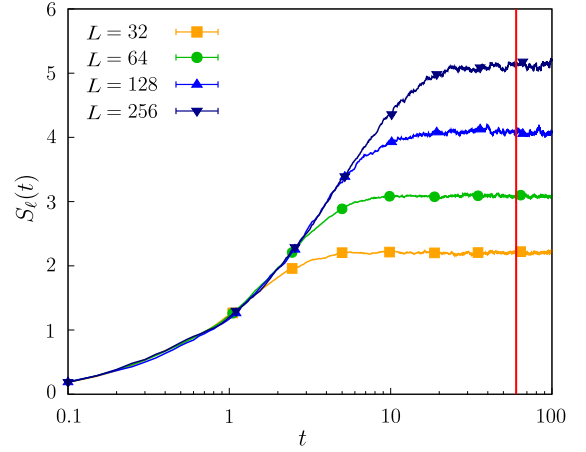


FIG. 2. Ensemble-averaged entanglement entropy as a function of time during a continuous measurement process, for different system sizes L , with $\ell = L/4$, $h_f = 1.0$, and $\gamma = 1.0$. The red line at $t = t^* = 60$ marks the time from which we evaluate the time-averaged entanglement entropy. Data are plotted in a semilog scale.

from subextensive to area-law growth with the global system size L ; the crossover point strongly depends on the system parameters.

We prepare the system in the ground-state of the Ising Hamiltonian (1) with a transverse field $h_i = +\infty$, and then we quench it to a value h_f finite. We monitor the dynamics of $S_\ell(t)$ for a subsystem of length $\ell = L/4$ [57]. $S_\ell(t)$ is a nonlinear function of the reduced density matrix, as discussed in Appendix D; we evaluate it over N_{rand} stochastic trajectories and then perform an ensemble average. For the rest of this paper, we set $N_{\text{rand}} = 100$ and, for quantum state diffusion, we take an integration step $\delta t = 0.05$ [58].

In Fig. 2 we show some prototypical trajectories of the entanglement entropy in time. The various colors refer to different system sizes, as indicated in the legend. The data have been taken with $h_f = 1$ and $\gamma = 1$, but the qualitative behavior is not affected by this specific choice: After a transient time $t^*(h_f, \gamma, L)$ that depends on the quench amplitude, the measurement rate, and the system size, the entanglement entropy reaches an asymptotic value that may obey a subvolume or an area-law behavior. We assume $t^* = 60$ (red line in Fig. 2), after a careful a-posteriori check that, for $t > t^*$, all the trajectories have converged to the asymptotic value.

We define the asymptotic entanglement entropy

$$\bar{S}_\ell = \lim_{T \rightarrow \infty} \frac{1}{T - t^*} \int_{t^*}^T dt S_\ell(t) \quad (15)$$

as the long-time-averaged entanglement entropy, where t^* is the transient time and T the total simulation time. The behavior of \bar{S}_ℓ is reported in Fig. 3, as a function of h_f and for different measurement rates γ . For small values of γ , the curves at different system sizes are well

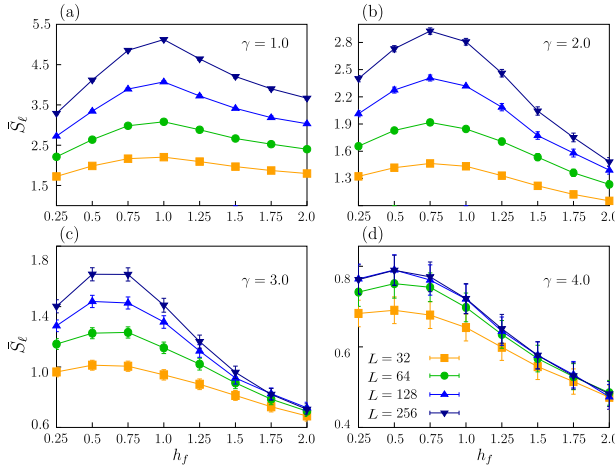


FIG. 3. Asymptotic entanglement entropy \bar{S}_ℓ (obtained by averaging over times larger than $t^* = 60$ —see red line in Fig. 2) as a function of the post-quench transverse field h_f for the measurement rates $\gamma = 1, 2, 3, 4$ [panels (a), (b), (c), (d), respectively]. The various colors correspond to different system sizes.

separated, thus suggesting a size-dependence of the entanglement entropy. As we will show later, this dependence agrees with the conformal scaling $\bar{S}_\ell(L) \sim \log(L)$. For larger γ values, even though the subextensive behavior survives when considering small system sizes and small transverse fields, a collapse of the curves emerges. We emphasize that the peak at $h_f \approx 1$, reminiscent of the unitary dynamics discussed in Sec. II A, appears for small values of γ in correspondence of the quantum critical point. Because of the competition between the Hamiltonian evolution and the non-conserving one, when increasing the measurement rate γ , this peak progressively shifts toward smaller transverse fields and eventually disappears. We remark that a similar behavior is observed in the ground-state entanglement of the quantum Ising chain at finite temperature [59].

Figure 4 displays the asymptotic entanglement entropy \bar{S}_ℓ as a function of the system size L (notice the logarithmic scale on the x axis), for different values of γ (cf. different panels) and h_f (cf. different colors). We distinguish two behaviors: Some trajectories show a logarithmic growth \bar{S}_ℓ with L . In this case, the data points follow a linear fit, whose slope determines the central charge of the associated conformal description. When increasing h_f , the trajectories bend to eventually settle on a constant value, i.e., an area-law behavior. The bending point, corresponding to the crossover point from the subextensive regime to the area-law one, strongly depends on h_f , γ and L . We define h_f^c as the critical transverse field where the crossover between area-law and logarithm-law takes place.

The dashed lines in the top panels of Fig. 4 are obtained by fitting the data up to $L_{\max} = 256$ with

$$f(L) \sim \tanh [\lambda(h_f, \gamma) \log(L)]. \quad (16)$$

In the bottom panels of Fig. 4 we show $\lambda(h_f, \gamma)$ as a function of h_f , for fixed γ . The color of each point refers to that of the corresponding trajectory in the associated top panels. Anytime the fit is reliable, the curve follows an hyperbolic tangent behavior, meaning that the entanglement entropy will eventually attain an area-law regime. The fit is not reliable when $\lambda L_{\max} \ll 1$ and the curve is indistinguishable from a straight line, suggesting a logarithm-law behavior. In practice, we consider the fit to be reliable whenever $\lambda(h_f, \gamma) \log L_{\max}$ is of order 1 or larger. Therefore we take the relation

$$\lambda(h_f^c, \gamma) \log L_{\max} \sim 1 \quad (17)$$

as a qualitative estimate of the crossover transverse field h_f^c for the given γ [this condition is marked by the red horizontal lines in Fig. 4(e-h)]. Hereafter, for simplicity of notation, we set $\lambda(h_f, \gamma) \equiv \lambda$.

In Fig. 1 we sketch the phase diagram obtained by carrying out the above analysis for two values of $L_{\max} = 192$ (small empty circles) and $L_{\max} = 256$ (big filled circles) [60]. We identify three regions in the phase diagram corresponding to an extensive, a subextensive, and an area-law regime. For $\gamma = 0$, the dynamics is unitary and the asymptotic entanglement entropy obeys a volume-law scaling. For $\gamma \geq 4$, the entanglement entropy follows an area-law, as predicted in Ref. [51]. For $0 < \gamma < 4$, there exists a critical line $h_f^c(L_{\max}, \gamma)$ dividing a region where the entanglement grows subextensively from another region where it exhibits an area-law scaling. We notice that the smaller the measurement rate γ , the higher the critical transverse field h_f^c . Moreover, at fixed γ , the critical transverse field reduces while increasing the system size. In principle, this leaves open the possibility that, in the thermodynamic limit, the subextensive region might eventually fade away, despite a numerical proof of this conjecture appears out of reach.

IV. QUANTUM JUMPS: RESULTS

We now compare the results in the previous section with those obtained by using a quantum-jump protocol. We put the emphasis on some discrepancies between the results obtained with the two unravelings (Sec. IV A). Finally, we compare the results of the stochastic evolutions with those coming from non-Hermitian Hamiltonian evolution, showing that this approximation does not capture many features of the entanglement entropy (Sec. IV B).

A. Jumps evolution

Let us consider the quantum-jump dynamics described in Sec. II B. We discretize the time in steps separated by δt and, at each time step, we extract a random number $r \in [0, 1]$. If $r > \sum_j \pi_j$ we do not perform any measure; otherwise, if $\pi_j < r \leq \pi_{j+1}$ we measure \hat{m}_j according

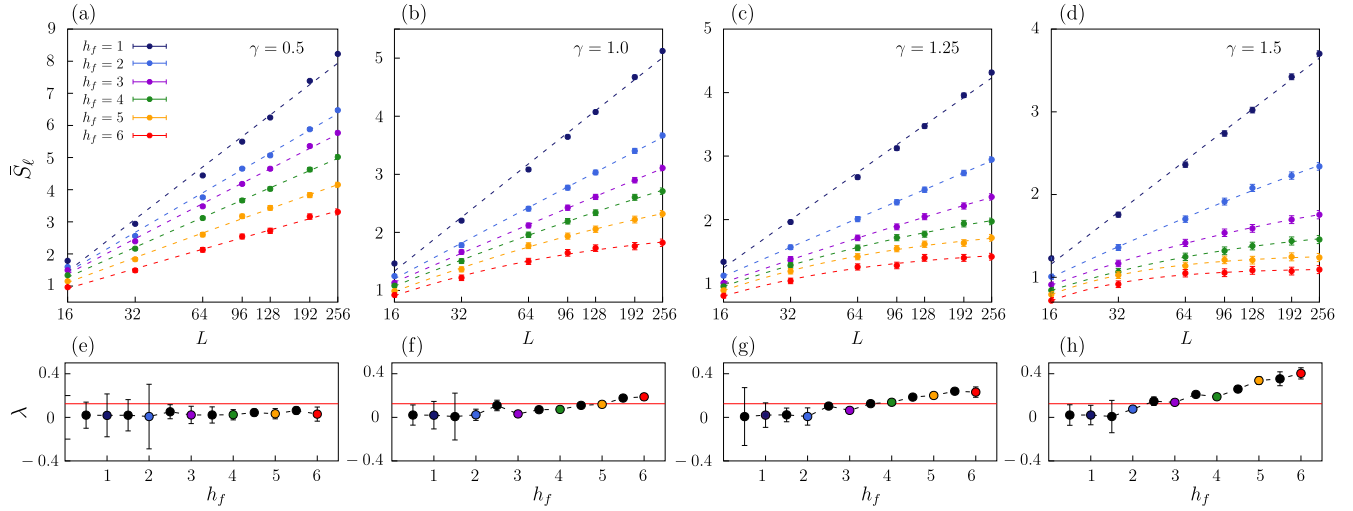


FIG. 4. Top panels: Asymptotic entanglement entropy \tilde{S}_L as a function of the system size L (in semilog scale) for several values of h_f (different colors), at fixed measurement rates $\gamma = 0.5, 1, 1.25, 1.5$ [panels (a), (b), (c), (d), respectively]. We identify two behaviors: either \tilde{S}_L grows logarithmically with L , or it settles on a constant value. The crossover between these two regimes locates a measurement-induced phase transition. Dashed lines are obtained by fitting the data up to the largest available size, $L_{\max} = 256$, with the function in Eq. (16). Bottom panels: λ as a function of h_f , for $\gamma = 0.5, 1.0, 1.25, 1.5$ [panels (e), (f), (g), (h), respectively]. The color of the points refers to the corresponding entanglement trajectory in the top panels. The red line highlights the value $1/\log L_{\max}$, corresponding to the validity bound of the fit: anytime $\lambda \log L_{\max}$ is of order 1 or larger, we consider the fit reliable and the curve follows a hyperbolic tangent behavior (i.e., the entanglement shows an area-law behavior). In contrast, for $\lambda \log L_{\max} \ll 1$ the behavior is indistinguishable from a straight line marking a subextensive scaling of the entanglement.

to Eq. (12). Attention must be paid in the choice of δt : In fact, if the time step is too large, the probabilities π_j might exceed one. After a convergence check, we fixed the time step $\delta t^{-1} \propto 8N\gamma\alpha$.

Although the dynamics is different from the quantum-state-diffusion one, we fix $\alpha = 1$ in order to recover the same master equation for the averaged density matrix. In Fig. 5 we show the entanglement entropy trajectories for $\gamma = 0.5, h_f = 0.5, 1.0, 2.0$, and various system sizes [panels (a), (b), (c), respectively]. Despite the differences in the asymptotic value, the entanglement entropy in time follows similar trajectories as those in Fig. 2. In Fig. 5(d) we plot the value of the asymptotic entanglement entropy \tilde{S}_L as a function of the system size L , showing that \tilde{S}_L is experiencing a logarithmic growth with L . We notice that the entanglement entropy for $h_f = 1.0$ is comparable with that at $h_f = 2.0$, suggesting a possible role of the ground-state critical point of the unitary dynamics also on the quantum-jump dynamics (we conjecture that, at fixed L and for h_f approaching h_c from the ferromagnetic phase, \tilde{S}_L grows, while it may not depend on h_f in the paramagnetic region).

Despite giving rise to the same Lindbladian, the quantum-jump dynamics does not provide the same phase diagram as the quantum diffusion protocol (Fig. 1). In all the cases we check, the scaling of the asymptotic entropy is logarithm-law [Fig. 5(d) and 6], also in the cases where the quantum diffusion provides an area-law scaling. To better clarify this point, we fix $\gamma = 1.5$ and pick up three representative points of the quantum diffusion

phase diagram, in the subextensive region ($h_f = 2.0$ – blue circle in Fig. 1), on the crossover line ($h_f = 5.0$ – orange circle in Fig. 1), and in the area-law phase ($h_f = 8.0$ – light-green circle), and we plot the asymptotic entropy versus L in 6. All the curves obey the logarithm-law. As a comparison, we also plot the same curves obtained at in the quantum state diffusion approximations (empty points and dashed lines). The curves for $h = 5.0, 8.0$ saturate, in contrast with the quantum-jump logarithmic growth obtained for the same parameters. From these data it is impossible to state whether the transition is suppressed (because of the choice of the unraveling or the jump operators) or if it shifts to different measurement rates and system sizes, due to limits in the numerically accessible system sizes.

B. Non-Hermitian Hamiltonian approximation

Finally, we consider the entanglement dynamics in the so-called *no-click limit*, meaning that the entanglement entropy is evaluated over post-selected trajectories that did not jump during the evolution. This class of trajectories follows a deterministic dynamics driven by the non-Hermitian Hamiltonian in Eq. (9). There are some results in the literature showing that sometimes it is possible to find a correspondence between the measurement-induced entanglement transition and the purely non-Hermitian dynamics [51, 61–63].

As an example, the authors of Ref. [51] show that the

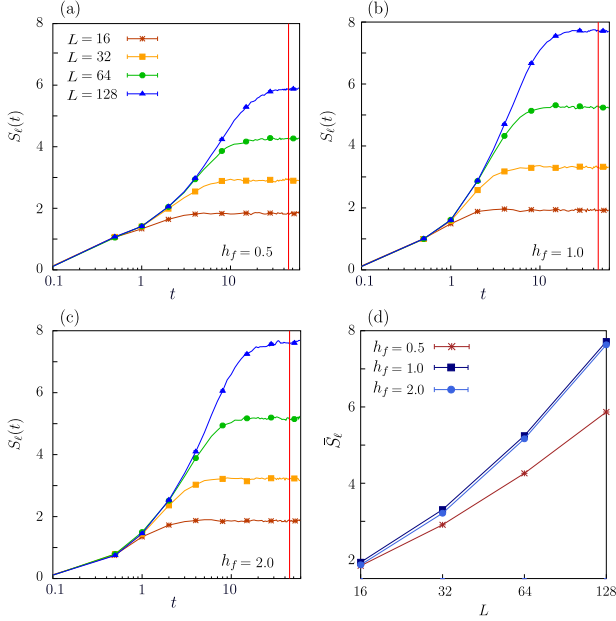


FIG. 5. Panels (a), (b), (c): Quantum-jump evolution of the entanglement entropy $S_\ell(t)$ for $\alpha = 1.0$ as a function of time, for $h_f = 0.5, 1.0, 2.0$ [panels (a), (b), (c), respectively] and $\gamma = 0.5$. The various colors correspond to different system sizes L . Panel (d) shows the asymptotic value \bar{S}_ℓ , obtained by averaging on times larger than $t^* = 160$ [cf. red line in panels (a), (b), (c)], for the three considered values of h_f , as a function of L (in semilog scale).

entanglement transition of the Ising chain in the absence of transverse field ($h = 0$) can be quantitatively located also by looking at the non-Hermitian dynamics of the entanglement entropy. This result is corroborated by some observations on the spectrum of Eq. (9),

$$\omega_k^{\text{n-H}}\left(h = \frac{i\gamma}{4}\right) = 2J\sqrt{1 - \frac{\gamma^2}{16J^2} - i\frac{\gamma}{2J}\cos k} \quad (18)$$

obtained by substituting $h = i\gamma/4$ in Eq. (4). In fact, the critical rate $\gamma_c = 4$ is the one at which the real part of the spectrum vanishes and the imaginary part becomes gapped. Despite this, the non-Hermitian evolution fails to predict the entanglement entropy dynamics, as soon as a finite transverse field is considered. To prove this, we simulate the non-Hermitian dynamics for quenches towards $h_f > 0$. In order to have the same non-Hermitian Hamiltonian of Ref. [51] and to simplify the comparison, for these simulations we set $\alpha(2 + \alpha) = 1$, i.e., $\alpha = \sqrt{2} - 1 \approx 0.41$. We point out that, even though the Lindblad equation for the averaged density matrix with $\alpha \sim 0.41$ is different from that considered in Subsec. II B, in the no-click limit the evolution of the state is fully determined by the non-Hermitian dynamics. We checked the non-Hermitian evolution with $\alpha = 1.0$ without finding qualitative differences with the other case.

In Figs. 7(a), 7(b), and 7(c) we show non-Hermitian evolution trajectories with the same parameters of

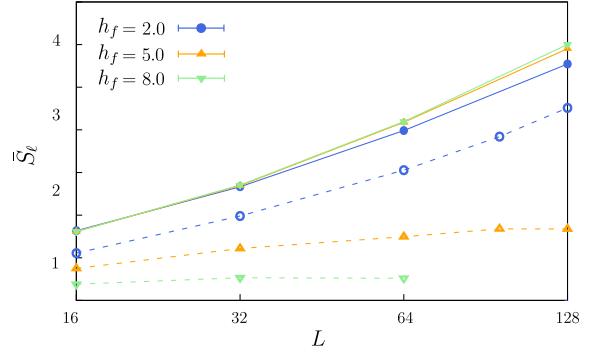


FIG. 6. Asymptotic entanglement entropy \bar{S}_ℓ as a function of the system size in the quantum-jump dynamics for $h_f = 2, 5, 8$, and $\gamma = 1.5$ (blue, orange, and light-green circles in Fig. 1, respectively). Notice that, even though $h_f = 5, 8$ correspond to the area-law phase in the quantum state diffusion phase diagram here the entanglement entropy exhibits a subextensive growth. For comparison, the empty dots show the same results obtained in the quantum state diffusion approximation.

Figs. 5(a), 5(b) and 5(c), respectively. We notice that not only the entanglement follows qualitatively different time traces, but also the convergence is much slower than in the quantum-jump case. In Fig. 7(d) we show the asymptotic entanglement entropy as a function of the system size for the three values of h_f considered so far. What emerges is that this approximate dynamics predicts a different entanglement scaling than the quantum state diffusion and the quantum jumps. For instance, while the curve at $h_f = 2.0$ in Fig. 7(d) is constant in L , the same curve obtained with the quantum-state-diffusion dynamics at the same γ grows logarithmically with L [Fig. 4(a)]. Moreover, the asymptotic entanglement entropy obtained from the non-Hermitian evolution is monotonous decreasing with h_f . As a consequence, we do not find any evidence of the critical point for small measurement rates, in contrast with the quantum-state-diffusion model [see Fig. 3]. Interestingly, the considerations done on the spectrum of the non-Hermitian Hamiltonian at $h_f = 0$ [51] cannot be extended to the case of a complex transverse field, namely $h_f > 0$. In fact, as it emerges by substituting $h = h_f + i\gamma/4$ in Eq. (4), it is not possible to find a k -independent γ that makes the real part of the spectrum vanishing, while keeping the imaginary part gapless.

V. DISCUSSION AND CONCLUSION

We focused on measurement-induced entanglement phase transitions in the quantum Ising chain, subject to different measurement processes resulting in the same Lindblad master equation for the averaged density matrix. We chose two different unraveling modeling measures: (i) the quantum-state-diffusion model, occur-

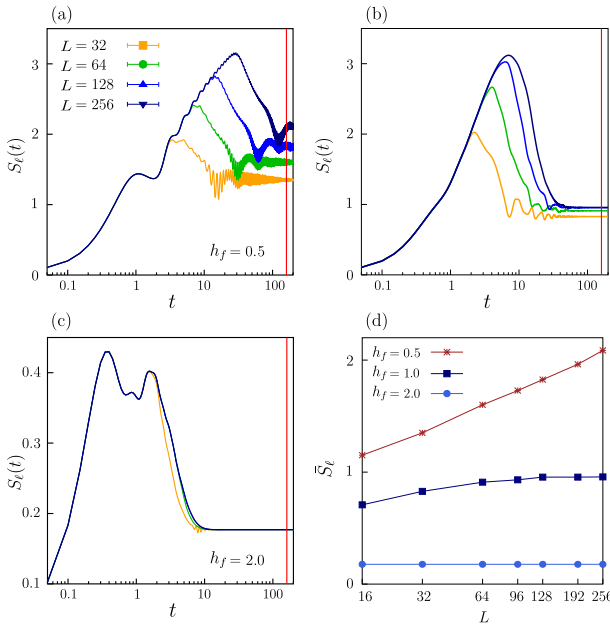


FIG. 7. Panels (a), (b), (c): Non-Hermitian evolution of the entanglement entropy $S_\ell(t)$ as a function of time, for $h_f = 0.5, 1.0, 2.0$ [panels (a), (b), (c), respectively], and $\gamma = 0.5$. The various colors correspond to different system sizes. Panel (d) shows the asymptotic value \bar{S}_ℓ [obtained by averaging on times larger than $t^* = 160$ —the red line in panels (a), (b), (c)] for the three h_f as a function of L . The curves in panel (a) show a larger transient than the others, therefore, before evaluating the \bar{S}_ℓ , we carefully checked for their behavior at later times.

ring weakly but continuously in time, and (ii) quantum-jump description, occurring abruptly but randomly in time. In doing this, to allow simulations for larger systems, we payed attention in choosing measurement operators which preserve the Gaussianity of the evolving quantum state.

From one side we found is that the quantum-state-diffusion dynamics predicts a crossover form a subextensive (logarithm-law) phase of the entanglement entropy to an area-law one. From the other side, the quantum-jump dynamics shows always a logarithm-law of the asymptotic entanglement entropy, and predicts no crossover, although the Lindblad equation is the same. As expected, we never recover the volume-law growth typical of the unitary evolution.

Our results emphasize the fact that the entanglement entropy is determined by the quantum correlations contained in the single quantum trajectory, that strongly depend on the choice of the unraveling. During the averaging process leading to the Lindblad equation, classical correlations appear as well. The resulting correlations in the averaged density matrix are of both types and cannot be disentangled from each other. Different unravelings provide different amounts of quantum correlations in the single quantum trajectories —and then different behaviors of the entropy— although the average density

matrix is always the same.

In this framework, different behaviors of entanglement come from the competition between unitary dynamics and measurement process. According to the environment measurement process over which the quantum-trajectory averaging is performed, the same Lindblad equation —and the same average density matrix— can come from a “more quantum” evolution, where the constructive effect of the unitary dynamics leads to large entanglement, or from a “more classical” one, where the destructive effect of the measurements prevails. The same competition gives rise to the transitions between different entanglement dynamical phases, when the unraveling is fixed and the coupling with the environment is varied (as occurs in the quantum-state-diffusion case).

However even though, to the best of our knowledge, for integrable fermionic models there are no examples of measurements preserving the volume-law scaling, some results in literature propose more complicated models displaying it, as for the case of measurements performed at discrete periodic times in ergodic phase [12] or in integrable MBL systems, provided appropriate measurement operators are chosen [36]. It would be tempting to check whether it is possible to find a set of continuously measured operators which can provide, in our framework, a volume-law asymptotic entanglement entropy. In this respect, an interesting possibility would be to exploit, for instance, long-range interactions in the definition of the measurement operators [64].

Finally, we mention that some recent experimental proposals for measuring the entanglement entropy [65, 66] in this kind of measurement-driven dynamics have been put forward [67–70] and realized [71]. Further experimental advances in this direction could help to open new directions in this field, shading some light on the problem of the unraveling dependence of entanglement transitions.

Note added: During the completion of this work, we became aware of a related manuscript [72] discussing the emergence of entanglement transitions in free-fermion models evolving under quantum jumps.

ACKNOWLEDGMENTS

We thank R. Fazio and R. Khasseh for useful discussions. We acknowledge support from the Italian MIUR through PRIN Project No. 2017E44HRF. The simulations have been carried using Armadillo c++ library [73, 74].

Appendix A: Diagonalization of the ising model

In this appendix we recall how to diagonalize the quantum Ising chain, described by the Hamiltonian in Eq. (1). First we introduce the Jordan-Wigner transformation,

$$\hat{\sigma}_j^+ = (e^{i\pi \sum_{\ell=1}^{j-1} \hat{n}_\ell}) \hat{c}_j^\dagger, \quad (A1)$$

where $\hat{\sigma}_j^\pm = \frac{1}{2}(\hat{\sigma}_j^x \pm i\hat{\sigma}_j^y)$ are the raising and lowering operators of the j th spin, that maps Eq. (1) into the spinless-fermion Hamiltonian

$$\hat{H} = -J \sum_{j=1}^{L-1} (\hat{c}_j^\dagger \hat{c}_{j+1} + \hat{c}_j^\dagger \hat{c}_{j+1}^\dagger + \text{h.c.}) + h \sum_{j=1}^L (2\hat{n}_j - 1) + (-1)^N J(\hat{c}_L^\dagger \hat{c}_1 + \hat{c}_L^\dagger \hat{c}_1^\dagger + \text{h.c.}). \quad (\text{A2})$$

In this expression, $\hat{c}_j^{(\dagger)}$ denote anticommuting fermionic annihilation (creation) operators, $\hat{n}_j = \hat{c}_j^\dagger \hat{c}_j$ is the corresponding local number operator, and $N = \sum_j \langle \hat{c}_j^\dagger \hat{c}_j \rangle$ is the total number of fermions. The last term in Eq. (A2) accounts for the periodic boundary conditions and, because of the highly non-local character of the transformation (A1), is strongly affected by the parity sector in which one is working. In our case we fix N even, hence we assume antiperiodic boundary conditions in Eq. A2. The Hamiltonian (A2) can be written in the compact form

$$\hat{H} = \frac{1}{2}\hat{\Psi}^\dagger \mathbb{H} \hat{\Psi} + \text{const.}, \quad (\text{A3})$$

where $\hat{\Psi} = (\hat{c}_1, \dots, \hat{c}_L, \hat{c}_1^\dagger, \dots, \hat{c}_L^\dagger)^T$ is the Nambu spinor introduced in the main text, while

$$\mathbb{H} = \begin{pmatrix} A & B \\ -B & -A \end{pmatrix} \quad (\text{A4})$$

is the so-called Bogoliubov-De Gennes Hamiltonian matrix, with entries

$$\begin{cases} A_{j,j} = h, & A_{j,j+1} = A_{j+1,j} = -J/2, \\ B_{j,j} = 0, & B_{j,j+1} = -B_{j+1,j} = -J/2, \\ A_{L,1} = A_{1,L} = B_{L,1} = -B_{1,L} = (-1)^{N+1}J/2. \end{cases} \quad (\text{A5})$$

We now define a set of new fermions $\hat{\gamma}_k$ ($k = 1, \dots, L$), obeying canonical anticommutation rules, as follows:

$$\hat{\gamma}_k = \sum_{j=1}^L (U_{jk}^* \hat{c}_j + V_{jk}^* \hat{c}_j^\dagger). \quad (\text{A6})$$

The associated Nambu spinor is given by $\hat{\Phi} = (\hat{\gamma}_1, \dots, \hat{\gamma}_L, \hat{\gamma}_1^\dagger, \dots, \hat{\gamma}_L^\dagger)^T = \mathbb{U}^\dagger \hat{\Psi}$, with

$$\mathbb{U} = \begin{pmatrix} U & V^* \\ V & U^* \end{pmatrix}. \quad (\text{A7})$$

The \mathbb{U} matrix implements the so-called Bogoliubov transformation, which makes the Hamiltonian diagonal in the γ_k fermions [cf. Eq. (3)], with a dispersion relation given by Eq. (4).

Appendix B: Continuous measurement dynamics

In this appendix we discuss more technical details of the dynamics in presence of continuous measurements.

As stated in the main text, the dynamics of these kind of measurements is captured by a collection of Wiener processes. A Wiener process is an ideal quantum walk with arbitrary small, independent, steps taken arbitrarily often, that is normally distributed with zero mean and variance growing linearly in time. The resulting stochastic Schrödinger equation reads

$$d|\psi_t\rangle = -i\hat{H}dt|\psi_t\rangle + \left\{ \sum_j \sqrt{\gamma}(\hat{n}_j - \langle \hat{n}_j \rangle) dW_t^j \right\} |\psi_t\rangle - \frac{1}{2} \left\{ \sum_j \gamma(\hat{n}_j - \langle \hat{n}_j \rangle)^2 dt \right\} |\psi_t\rangle, \quad (\text{B1})$$

with W_t^j independent Wiener processes. By Trotterizing Eq. (B1), we obtain the approximate evolution in Eq. (7).

For a Gaussian state, this evolution reduces to that of the correlation matrices U, V defined in Eq. (A7). In particular, it can be written as a two-step evolution driven first by the Hamiltonian part, which is given by the unitary transformation

$$\begin{bmatrix} U'(t + \delta t) \\ V'(t + \delta t) \end{bmatrix} = e^{-2i\mathbb{H}\delta t} \begin{bmatrix} U(t) \\ V(t) \end{bmatrix}, \quad (\text{B2})$$

and then by the dissipative part

$$\mathbb{W} = \exp \begin{bmatrix} T & 0 \\ 0 & -T \end{bmatrix} \begin{bmatrix} U'(t + \delta t) & (V'(t + \delta t))^* \\ V'(t + \delta t) & (U'(t + \delta t))^* \end{bmatrix}, \quad (\text{B3})$$

where T is a $L \times L$ diagonal matrix defined as

$$T_{jj} = \delta W_t^j + (2\langle \hat{n}_j \rangle_t - 1)\gamma \delta t. \quad (\text{B4})$$

Since the dissipative part does not conserve the norm of the state, to keep it normalized we have to perform a QR decomposition $\mathbb{W} = \mathbb{Q} \cdot \mathbb{R}$, with \mathbb{Q} an orthogonal matrix and \mathbb{R} an upper triangular one. Thus the time-evolved state is simply $\mathbb{U}(t + \delta t) \equiv \mathbb{Q}$. [11, 51]

Appendix C: Quantum jumps dynamics

In this appendix we give some technical details on the quantum jump evolution described in the main text. This protocol is quite different from the continuous measurement one. The main difference in the presence of measurements of the local number of fermions \hat{n}_j is that Gaussianity is not preserved anymore. To show this, we exploit the operator identity

$$\hat{n}_j = \frac{e^{x\hat{n}_j} - 1}{e^x - 1}. \quad (\text{C1})$$

As explained in the main text, during the dynamics, the system evolution is obtained by applying either the non-Hermitian Hamiltonian or the jump operator that, in this case, we assume to be \hat{n}_j . From Eq. (C1), it is easy to notice that by applying \hat{n}_j to a Gaussian state we obtain a superposition of two Gaussian states, that is not

guaranteed to remain Gaussian. We can overcome this problem by choosing the jump operators $\hat{m}_j = \sqrt{\gamma}(\hat{1} + \alpha\hat{n}_j)$ defined in Eq. (10). In fact, once fixed $x = \log(1 + \alpha)$, we have

$$\hat{m}_j = \sqrt{\gamma} \left(\hat{1} + \alpha \frac{e^{x\hat{n}_j} - 1}{e^x - 1} \right) = \sqrt{\gamma} e^{x\hat{n}_j}. \quad (\text{C2})$$

This quantum-jump dynamics is well described by the stochastic equation

$$\begin{aligned} d|\psi_t\rangle = -i\hat{H}dt|\psi_t\rangle - \frac{\gamma}{2} \left\{ \sum_j (\hat{m}_j - \langle \hat{m}_j \rangle) dt \right\} |\psi_t\rangle \\ + \left\{ \sum_j \left(\frac{\hat{m}_j}{\sqrt{\langle \hat{m}_j \rangle_t}} - 1 \right) dN_t^j \right\} |\psi_t\rangle, \end{aligned} \quad (\text{C3})$$

where N_t are Poisson processes with $dN_t^j = 0, 1$, $(dN_t^j)^2 = dN_t^j$ and $dN_t^j = \gamma dt \langle n_j \rangle_t$. The evolution driven by the non-Hermitian Hamiltonian in Eq. (9) is obtained by solving the equation

$$i \frac{d}{dt} \begin{bmatrix} U(t) \\ V(t) \end{bmatrix} = 2 \mathbb{H}_{\text{eff}} \begin{bmatrix} U(t) \\ V(t) \end{bmatrix}, \quad (\text{C4})$$

with \mathbb{H}_{eff} the non-Hermitian Bogoliubov De-Gennes Hamiltonian (defined in analogy with the Hermitian one). The exponential operator $\hat{m}_j = e^{x\hat{n}_j}$ can be applied to a Gaussian state by simply applying to \mathbb{U} the matrix \mathbb{M} , which is defined as follows:

$$\begin{cases} \mathbb{M}_{i,i} = 1 & \text{for } i \neq j, j+L, \\ \mathbb{M}_{j,j} = \mathbb{M}_{j+L,j+L}^{-1} = e^x, \end{cases} \quad (\text{C5})$$

Appendix D: Entanglement entropy in fermionic Gaussian states

The entanglement entropy of a subsystem of dimension ℓ is defined as

$$S_\ell = -\rho_\ell \log \rho_\ell, \quad \text{with } \rho_\ell(t) = \text{Tr}_{L/\ell} [\rho_L(t)] \quad (\text{D1})$$

being the reduced density matrix of the subsystem. Finding $\rho_\ell(t)$ is usually a computationally hard task, in particular for spin systems whose Hilbert space grows exponentially with the system size L . Luckily, when dealing with Gaussian states (such as in the case of the Ising chain) the possibility of exploiting Wick's theorem remarkably reduces the computational effort. In fact, it is possible to write ρ_ℓ by defining ℓ appropriate uncorrelated fermionic operators [46, 75]. Below we provide details on the procedure to follow to write down these operators.

First, we need the $2L \times 2L$ correlation matrix

$$\mathbb{G}(t) = \mathbb{U}(t) \left(\begin{array}{c|c} \mathbb{I} & 0 \\ \hline 0 & 0 \end{array} \right) \mathbb{U}^\dagger(t) = \left(\begin{array}{c|c} G(t) & F(t) \\ \hline F^\dagger(t) & 1 - G^T(t) \end{array} \right), \quad (\text{D2})$$

with $G_{jj'}(t) \equiv \langle \hat{c}_j \hat{c}_{j'}^\dagger \rangle_t$ and $F_{jj'}(t) \equiv \langle \hat{c}_j \hat{c}_{j'} \rangle_t$. We now introduce the Majorana fermions

$$\check{c}_{j,1} = \hat{c}_j^\dagger + \hat{c}_j, \quad \check{c}_{j,2} = i(\hat{c}_j^\dagger - \hat{c}_j). \quad (\text{D3})$$

Analogously to the Nambu spinors, the Majorana column vector is defined as $\check{\mathbf{c}} = (\check{c}_{1,1}, \dots, \check{c}_{L,1}, \check{c}_{1,2}, \dots, \check{c}_{L,2})^T$, through the relation

$$\check{\mathbf{c}} = \mathbb{W} \hat{\mathbf{c}}, \quad \text{with } \mathbb{W} = \left(\begin{array}{c|c} \mathbb{I} & \mathbb{I} \\ \hline -i\mathbb{I} & i\mathbb{I} \end{array} \right). \quad (\text{D4})$$

Using this relation, we can evaluate the Majorana correlation matrix $\mathbb{M}_{nn'}(t) = \langle \check{c}_n \check{c}_{n'} \rangle$ as:

$$\mathbb{M}(t) = \mathbb{W} \mathbb{G}(t) \mathbb{W}^\dagger. \quad (\text{D5})$$

We can decompose the matrix $\mathbb{M}(t) = \mathbb{I} + i\mathbb{A}(t)$. The reduced Majorana correlation matrix \mathbb{M}^ℓ can be then constructed according to

$$\begin{cases} \mathbb{M}_{n,n'}^\ell = \delta_{n,n'} + i\mathbb{A}_{n,n'}, \\ \mathbb{M}_{n,l+n'}^\ell = i\mathbb{A}_{n,L+n'} \\ \mathbb{M}_{l+n,n'}^\ell = i\mathbb{A}_{L+n,n'}, \\ \mathbb{M}_{l+n,l+n'}^\ell = \delta_{n,n'} + i\mathbb{A}_{L+n,L+n'}, \end{cases} \quad (\text{D6})$$

with $n, n' \in \{1, \dots, \ell\}$.

At each time step t , one can transform the matrix $\mathbb{A}^\ell(t)$ to a canonical form, by a (real) orthogonal transformation \mathbb{R} (Schur's decomposition)

$$\mathbb{A}_\ell(t) = \mathbb{R}(t) \tilde{\mathbb{A}}(t) \mathbb{R}^\dagger(t), \quad \text{with } \tilde{\mathbb{A}} = \bigoplus_{q=1}^{\ell} \begin{pmatrix} 0 & \lambda_q \\ -\lambda_q & 0 \end{pmatrix}. \quad (\text{D7})$$

This rotation defines a new (non local) combination of Majorana fermions $\check{d}_q = \sum_{n=1}^{2\ell} \mathbb{R}_{nq}(t) \check{c}_n$. Transforming back and defining ℓ fermionic operators $\hat{d}_q = \mathbb{W}^{-1} \check{d}_q$, it can be shown that, in this basis, the reduced density matrix factorizes in ℓ blocks of size 2×2 , having eigenvalues

$$P_q(t) = \frac{1 + \lambda_q(t)}{2}, \quad 1 - P_q(t) = \frac{1 - \lambda_q(t)}{2}. \quad (\text{D8})$$

The entanglement entropy is thus given by

$$S_\ell(t) = - \sum_{q=1}^{\ell} P_q(t) \log P_q(t) + [1 - P_q(t)] \log [1 - P_q(t)]. \quad (\text{D9})$$

[1] R. P. Feynman and F. L. Vernon, The theory of a general quantum system interacting with a linear dissipative system, *Ann. Phys.* **24**, 118 (1963).

[2] A. J. Leggett, Quantum Mechanics at the Macroscopic Level, in *Le hasard et la matière/Chance and matter*, Les Houches, Session XLVI, 1986, edited by J. Souletie and J. Vannimenus and R. Stora (Elsevier Science, 1987).

[3] W. J. Zurek, Decoherence, einselection, and the quantum origins of the classical, *Rev. Mod. Phys.* **75**, 715 (2003).

[4] D. Manzano, A short introduction to the lindblad master equation, *AIP Advances* **10**, 025106 (2020).

[5] B.-G. Englert and G. Morigi, Five lectures on dissipative master equations, *Lecture Notes in Physics* , 55–106 (2002).

[6] H.-P. Breuer, F. Petruccione, *et al.*, *The theory of open quantum systems* (Oxford University Press on Demand, 2002).

[7] A. J. Daley, Quantum trajectories and open many-body quantum systems, *Adv. Phys.* **63**, 77 (2014).

[8] M. B. Plenio and P. L. Knight, The quantum-jump approach to dissipative dynamics in quantum optics, *Rev. Mod. Phys.* **70**, 101 (1998).

[9] L. Amico, R. Fazio, A. Osterloh, and V. Vedral, Entanglement in many-body systems, *Rev. Mod. Phys.* **80**, 517 (2008).

[10] M. A. Nielsen and I. L. Chuang, *Quantum Computation and Quantum Information: 10th Anniversary Edition*, 10th ed. (Cambridge University Press, New York, NY, USA, 2011).

[11] X. Cao, A. Tilloy, and A. D. Luca, Entanglement in a fermion chain under continuous monitoring, *SciPost Phys.* **7**, 24 (2019).

[12] B. Skinner, J. Ruhman, and A. Nahum, Measurement-induced phase transitions in the dynamics of entanglement, *Phys. Rev. X* **9**, 031009 (2019).

[13] A. Chan, R. M. Nandkishore, M. Pretko, and G. Smith, Unitary-projective entanglement dynamics, *Phys. Rev. B* **99**, 224307 (2019).

[14] M. Szyniszewski, A. Romito, and H. Schomerus, Entanglement transition from variable-strength weak measurements, *Phys. Rev. B* **100**, 064204 (2019).

[15] Y. Fuji and Y. Ashida, Measurement-induced quantum criticality under continuous monitoring, *Phys. Rev. B* **102**, 054302 (2020).

[16] S. Goto and I. Danshita, Measurement-induced transitions of the entanglement scaling law in ultracold gases with controllable dissipation, *Phys. Rev. A* **102**, 033316 (2020).

[17] O. Lunt and A. Pal, Measurement-induced entanglement transitions in many-body localized systems, *Phys. Rev. Research* **2**, 043072 (2020).

[18] A. Nahum and B. Skinner, Entanglement and dynamics of diffusion-annihilation processes with majorana defects, *Phys. Rev. Research* **2**, 023288 (2020).

[19] N. Lang and H. P. Büchler, Entanglement transition in the projective transverse field ising model, *Phys. Rev. B* **102**, 094204 (2020).

[20] O. Alberton, M. Buchhold, and S. Diehl, Entanglement transition in a monitored free-fermion chain: From extended criticality to area law, *Phys. Rev. Lett.* **126**, 170602 (2021).

[21] T. Botzung, S. Diehl, and M. Müller, Engineered dissipation induced entanglement transition in quantum spin chains: from logarithmic growth to area law (2021), [arXiv:2106.10092 \[quant-ph\]](https://arxiv.org/abs/2106.10092).

[22] M. Coppola, E. Tirrito, D. Karevski, and M. Collura, Growth of entanglement entropy under local projective measurements (2021), [arXiv:2109.10837 \[cond-mat.stat-mech\]](https://arxiv.org/abs/2109.10837).

[23] Y. Li, X. Chen, and M. P. A. Fisher, Quantum zeno effect and the many-body entanglement transition, *Phys. Rev. B* **98**, 205136 (2018).

[24] Y. Li, X. Chen, and M. P. A. Fisher, Measurement-driven entanglement transition in hybrid quantum circuits, *Phys. Rev. B* **100**, 134306 (2019).

[25] M. J. Gullans and D. A. Huse, Scalable probes of measurement-induced criticality, *Phys. Rev. Lett.* **125**, 070606 (2020).

[26] C.-M. Jian, Y.-Z. You, R. Vasseur, and A. W. W. Ludwig, Measurement-induced criticality in random quantum circuits, *Phys. Rev. B* **101**, 104302 (2020).

[27] A. Zabalo, M. J. Gullans, J. H. Wilson, S. Gopalakrishnan, D. A. Huse, and J. H. Pixley, Critical properties of the measurement-induced transition in random quantum circuits, *Phys. Rev. B* **101**, 060301 (2020).

[28] S. Choi, Y. Bao, X.-L. Qi, and E. Altman, Quantum error correction in scrambling dynamics and measurement-induced phase transition, *Phys. Rev. Lett.* **125**, 030505 (2020).

[29] Y. Bao, S. Choi, and E. Altman, Theory of the phase transition in random unitary circuits with measurements, *Phys. Rev. B* **101**, 104301 (2020).

[30] L. Zhang, J. A. Reyes, S. Kourtis, C. Chamon, E. R. Mucciolo, and A. E. Ruckenstein, Nonuniversal entanglement level statistics in projection-driven quantum circuits, *Phys. Rev. B* **101**, 235104 (2020).

[31] M. Szyniszewski, A. Romito, and H. Schomerus, Universality of entanglement transitions from stroboscopic to continuous measurements, *Phys. Rev. Lett.* **125**, 210602 (2020).

[32] X. Turkehi, R. Fazio, and M. Dalmonte, Measurement-induced criticality in (2+1)-dimensional hybrid quantum circuits, *Phys. Rev. B* **102**, 014315 (2020).

[33] Y. Li, X. Chen, A. W. W. Ludwig, and M. P. A. Fisher, Conformal invariance and quantum nonlocality in critical hybrid circuits, *Phys. Rev. B* **104**, 104305 (2021).

[34] Y. Li and M. P. A. Fisher, Statistical mechanics of quantum error correcting codes, *Phys. Rev. B* **103**, 104306 (2021).

[35] R. Fan, S. Vijay, A. Vishwanath, and Y.-Z. You, Self-organized error correction in random unitary circuits with measurement, *Phys. Rev. B* **103**, 174309 (2021).

[36] O. Lunt, M. Szyniszewski, and A. Pal, Measurement-induced criticality and entanglement clusters: A study of one-dimensional and two-dimensional clifford circuits, *Phys. Rev. B* **104**, 155111 (2021).

[37] A. Lavasani, Y. Alavirad, and M. Barkeshli, Measurement-induced topological entanglement transitions in symmetric random quantum circuits, *Nat. Phys.* **17**, 342 (2021).

[38] S. Sang and T. H. Hsieh, Measurement-protected quantum phases, *Phys. Rev. Research* **3**, 023200 (2021).

[39] O. Shtanko, Y. A. Kharkov, L. P. García-Pintos, and A. V. Gorshkov, Classical models of entanglement in monitored random circuits (2020), [arXiv:2004.06736 \[cond-mat.dis-nn\]](https://arxiv.org/abs/2004.06736).

[40] A. Lavasani, Y. Alavirad, and M. Barkeshli, Topological order and criticality in $(2+1)d$ monitored random quantum circuits (2020), [arXiv:2011.06595 \[cond-mat.stat-mech\]](https://arxiv.org/abs/2011.06595).

[41] B. Shi, X. Dai, and Y.-M. Lu, Entanglement negativity at the critical point of measurement-driven transition (2020), [arXiv:2012.00040 \[cond-mat.stat-mech\]](https://arxiv.org/abs/2012.00040).

[42] M. Block, Y. Bao, S. Choi, E. Altman, and N. Yao, The measurement-induced transition in long-range interacting quantum circuits (2021), [arXiv:2104.13372 \[quant-ph\]](https://arxiv.org/abs/2104.13372).

[43] A. C. Potter and R. Vasseur, Entanglement dynamics in hybrid quantum circuits (2021), [arXiv:2111.08018 \[quant-ph\]](https://arxiv.org/abs/2111.08018).

[44] M. Fagotti and P. Calabrese, Evolution of entanglement entropy following a quantum quench: Analytic results for the hexychain in a transverse magnetic field, *Phys. Rev. A* **78**, 010306 (2008).

[45] P. Calabrese and J. Cardy, Evolution of entanglement entropy in one-dimensional systems, *J. Stat. Mech.* **2005**, P04010 (2005).

[46] G. Vidal, J. I. Latorre, E. Rico, and A. Kitaev, Entanglement in quantum critical phenomena, *Phys. Rev. Lett.* **90**, 227902 (2003).

[47] X. Chen, Y. Li, M. P. A. Fisher, and A. Lucas, Emergent conformal symmetry in nonunitary random dynamics of free fermions, *Phys. Rev. Research* **2**, 033017 (2020).

[48] Q. Tang and W. Zhu, Measurement-induced phase transition: A case study in the nonintegrable model by density-matrix renormalization group calculations, *Phys. Rev. Research* **2**, 013022 (2020).

[49] Y. Bao, S. Choi, and E. Altman, Symmetry enriched phases of quantum circuits, *Ann. Phys.*, 168618 (2021).

[50] M. Buchhold, Y. Minoguchi, A. Altland, and S. Diehl, Effective theory for the measurement-induced phase transition of dirac fermions, *Phys. Rev. X* **11**, 041004 (2021).

[51] X. Turkeshi, A. Biella, R. Fazio, M. Dalmonte, and M. Schirò, Measurement-induced entanglement transitions in the quantum ising chain: From infinite to zero clicks, *Phys. Rev. B* **103**, 224210 (2021).

[52] S. Sachdev, *Quantum phase transitions* (Cambridge university press, 2011).

[53] P. Calabrese and J. Cardy, Entanglement entropy and quantum field theory, *J. Stat. Mech.* **2004**, P06002 (2004).

[54] G. B. Mbeng, A. Russomanno, and G. E. Santoro, The quantum ising chain for beginners (2020), [arXiv:2009.09208 \[quant-ph\]](https://arxiv.org/abs/2009.09208).

[55] Hereafter, unless specified, summations over the site indexes j are intended to run over all the spins of the chain.

[56] “Small” means much smaller than the time scale of the resulting Lindblad dynamics, whose order of magnitude is $1/\gamma$ in Eq. (6) [8?].

[57] We have chosen $\ell = L/4$ for computational convenience. However we carefully checked that, in the thermodynamic limit, our results qualitatively depend only on the system size and not on the subsystem one.

[58] Such values of N_{rand} and δt have been selected after careful testing that the numerical errors introduced by these cutoffs are not affecting the results, on the scales of the figures presented in this work.

[59] L. Amico and D. Patanè, Entanglement crossover close to a quantum critical point, *Europhys. Lett.* **77**, 17001 (2007).

[60] Unfortunately, our computational resources did not allow us to go beyond $L_{\text{max}} = 256$, therefore we cannot establish whether and how h_f^c would change for larger values of L_{max} and, ultimately, in the thermodynamic limit.

[61] A. Biella and M. Schirò, Many-body quantum zeno effect and measurement-induced subradiance transition, *Quantum* **5**, 528 (2021).

[62] S. Gopalakrishnan and M. J. Gullans, Entanglement and purification transitions in non-hermitian quantum mechanics, *Physical Review Letters* **126**, 10.1103/physrevlett.126.170503 (2021).

[63] Z.-Y. Zhou, Z.-L. Xiang, J. Q. You, and F. Nori, Work statistics in non-hermitian evolutions with hermitian endpoints, *Phys. Rev. E* **104**, 034107 (2021).

[64] P. Sierant, G. Chiriacò, F. M. Surace, S. Sharma, X. Turkeshi, M. Dalmonte, R. Fazio, and G. Pagano, Dissipative floquet dynamics: from steady state to measurement induced criticality in trapped-ion chains (2021), [arXiv:2107.05669 \[quant-ph\]](https://arxiv.org/abs/2107.05669).

[65] R. Islam, R. Ma, P. M. Preiss, M. E. Tai, A. Lukin, M. Rispoli, and M. Greiner, Measuring entanglement entropy in a quantum many-body system, *Nature* **528**, 77 (2015).

[66] T. Brydges, A. Elben, P. Jurcevic, B. Vermersch, C. Maier, B. P. Lanyon, P. Zoller, R. Blatt, and C. F. Roos, Probing rényi entanglement entropy via randomized measurements, *Science* **364**, 260–263 (2019).

[67] T. Elliott, W. Kozlowski, S. Caballero-Benitez, and I. Mekhov, Multipartite entangled spatial modes of ultracold atoms generated and controlled by quantum measurement, *Physical Review Letters* **114**, 10.1103/physrevlett.114.113604 (2015).

[68] A. Elben, R. Kueng, H.-Y. R. Huang, R. van Bijnen, C. Kokail, M. Dalmonte, P. Calabrese, B. Kraus, J. Preskill, P. Zoller, and et al., Mixed-state entanglement from local randomized measurements, *Physical Review Letters* **125**, 10.1103/physrevlett.125.200501 (2020).

[69] M. Rossi, L. Mancino, G. T. Landi, M. Paternostro, A. Schliesser, and A. Belenchia, Experimental assessment of entropy production in a continuously measured mechanical resonator, *Physical Review Letters* **125**, 10.1103/physrevlett.125.080601 (2020).

[70] S. Czischek, G. Torlai, S. Ray, R. Islam, and R. G. Melko, Simulating a measurement-induced phase transition for trapped ion circuits (2021), [arXiv:2106.03769 \[quant-ph\]](https://arxiv.org/abs/2106.03769).

[71] C. Noel, P. Niroula, D. Zhu, A. Risinger, L. Egan, D. Biswas, M. Cetina, A. V. Gorshkov, M. J. Gullans, D. A. Huse, and C. Monroe, Observation of measurement-induced quantum phases in a trapped-ion quantum computer (2021), [arXiv:2106.05881 \[quant-ph\]](https://arxiv.org/abs/2106.05881).

[72] X. Turkeshi, M. Dalmonte, R. Fazio, and M. Schirò, Entanglement transitions from stochastic resetting of non-hermitian quasiparticles (2021), [arXiv:2111.03500 \[cond-mat.stat-mech\]](https://arxiv.org/abs/2111.03500).

[73] C. Sanderson and R. Curtin, A user-friendly hybrid sparse matrix class in c++, in *International Congress on Mathematical Software* (Springer, 2018) pp. 422–430.

[74] C. Sanderson and R. Curtin, Armadillo: a template-based c++ library for linear algebra, *Journal of Open Source Software* **1**, 26 (2016).

[75] J. I. Latorre, E. Rico, and G. Vidal, Ground state entanglement in quantum spin chains, *Quantum Inf. Comput.* **4**, 48 (2004).